The effect of gamma irradiation on $CaO\text{-}Fe_xO_y\text{-}SiO_2$ slag based inorganic polymers

Bram Mast[a*], Andrea Cambriani[b], Alexios P. Douvalis[c], Isabelle Gerardy[d], Grazyna Gryglewicz[e], Yiannis Pontikes[f], Wouter Schroeyers[a], Bram Vandoren[g], Sonja Schreurs[a**]

[a] Hasselt University, CMK, NuTeC, Nuclear Technology - Faculty of Engineering Technology, Agoralaan Building H, B-3590 Diepenbeek, Belgium
[b] European Commission, Joint Research Centre, P.O. Box 2340, D-76125 Karlsruhe, Germany
[c] University of Ioannina, Department of Physics, 45110 Ioannina, Greece
[d] Haute Ecole Bruxelles-Brabant HE2B, ISIB, Engineering Education Institute, Physical and Nuclear Department, Koningsstraat 150, B-1000 Brussels, Belgium
[e] Wrocław University of Science and Technology, Faculty of Chemistry, Department of Polymer and Carbonaceous Materials, Gdańska 7/9, 50-344 Wrocław, Poland
[f] KU Leuven, Department of Materials Engineering, Kasteelpark Arenberg 44, 3001 Heverlee, Belgium
[g] Hasselt University, CERG, Faculty of Engineering Technology, Agoralaan Building H, B-3590 Diepenbeek, Belgium

[*] Main Author, E-mail: bram.mast@uhasselt.be
[**] Corresponding Author: sonja.schreurs@uhasselt.be

ABSTRACT

Alternative cementitious materials to the commonly used ordinary Portland cement are being increasingly studied for radioactive waste encapsulation. In this view, geopolymers and inorganic polymers (IPs) have received wide attention. The absence of portlandite, the low water content and the high alkalinity, make IPs interesting candidates for the conditioning of certain radioactive waste streams. Moreover, Fe-rich IPs offer an interesting alternative to high density concretes for use in radiation shielding applications. Materials can however be altered when subjected to ionizing radiation, creating the necessity to study the material's behavior under irradiation conditions. In this study, the effect of gamma irradiation is investigated on $CaO\text{-}Fe_xO_y\text{-}SiO_2$ slag-based IPs. Samples with different curing times (1 h, 24 h and 28 days) prior to the irradiation were irradiated at different dose rates varying from 1.52 Gy/h to 8.85 kGy/h resulting in doses varying from 137 Gy to 715 kGy. For each irradiation test, non-irradiated samples were kept as a reference at the same environmental conditions as the irradiated samples. The results were also compared with studies on OPC-based samples.

The effect of gamma irradiation is observed to be highly dependent on the curing time prior to irradiation. The mechanisms behind the effects of irradiation are different for the non-hardened samples compared to hardened samples. Multiple effects were observed: a change in macroscopic strength, a change in porosity, radiation-altered carbonation, a decrease in water content and increase in $Fe^{3+}/\Sigma Fe$ ratio.

Introduction

For some decades, alternatives to the commonly used ordinary Portland cement (OPC) matrices are increasingly being studied. **Inorganic Polymers (IPs)** are one of the alternatives currently studied. IPs encompass a broad range of binder systems formed by the reaction of an alkali metal source (solid or dissolved) with a solid amorphous powdered precursor [1]. A three-dimensional-tetrahedral network is formed in which the aluminates and silicates are covalently bonded by shared oxygen atoms [2]. The alkali source can be any solid or solution which can raise the pH of the reaction mixture and dissolve the precursor [1].

The **chemistry** of alkali-activation can be summarized in four steps: (i) dissolution, (ii) reorganization, (iii) nucleation and (iv) polymerization and hardening [3]. In the first step, the ionic and covalent bonds are broken at the surface of the precursor material in contact with the high alkaline solution. Next, the diffusion of the alkali solution will bring more Al^{3+} and Si^{4+} into solution. In the alkaline environment, the alumina and silica forms monomeric tetrahedral structures of $Al(OH)_4)^-$ and $Si(OH)_4$). Due to polycondensation reactions, the gel will harden with the formation of an amorphous 3D network of Al-O-Si chains. In this structure, each Al- and Si-atom is bonded to four oxygen atoms. The resulting negative charge is compensated by the cations present in the activation solution (e.g. Na^+, K^+, Li^+, Ca^{2+}, Ba^{2+}, NH_4^+, H_3O^+). Moreover, recent study of Peys et al. [4] indicated the participation of Fe in the silicate network which enables the use of Fe-rich precursors for AAM production. Slags originating from nonferrous metallurgical industries which are currently underutilized can thus be used as a precursor for IP production [4]. Although the process is summarized in four steps, it should be mentioned that the different steps occur simultaneously [5], [6]. At the end, a three-phase material is formed consisting out of pores, binder and aggregates of which the binder is reacted precursor material and the aggregates are unreacted precursor particles.

Alkali activation technology has been recognized to offer high potential for immobilization of hazardous components [7], [8]. The high pH of the materials insolubilizes many metals and radioelements such as ^{137}Cs and protects metals from corrosion effects [9], [10], [11]. Additionally, these binders have **promising properties** as high chemical and temperature resistance [2], [12], making them interesting candidates for application in nuclear safety structures. IPs can be designed to have a low water content and thus generate less radiolytic hydrogen gas compared to OPC based matrices [9], [13]. IPs based on slags show high potential for use as gamma shielding material. High linear attenuation coefficients can be obtained using cheap slags, avoiding expensive aggregates currently used to produce high density concretes [14]. Fayalite slag based IPs were proven to have a similar gamma shielding capacity to basalt-magnetite concretes [14]. Also for neutron shielding, IPs form an interesting opportunity since boron can be incorporated in the matrix as a substituent of aluminum [15]. Moreover, IPs lose less water in time in comparison to fresh OPC samples what creates the possibility to easily design IPs with better neutron shielding capacities compared to aged concrete [16].

This work focusses on the effects of gamma irradiation on inorganic polymers. The effect of gamma irradiation is investigated on iron-rich CaO-FeO_x-SiO_2 slag-based IPs.

Material and Methods

Plasma slag has been chosen as resource material for the IP production in this study. This slag falls into a large group of non-ferrous metallurgy residues with a high iron content. When the slag is rapidly cooled, the resulting granulates are highly amorphous [17], making it a good candidate for IP production. The glass was milled using a ball mill until a Blaine value of (2.68 ± 0.02) · 10^3 cm^2/g according to EN 196-6 [18] before alkali activation. The chemical composition of the synthetic plasma slag was determined using X-ray fluorescence analysis (Bruker AXS S8 TIGER spectrometer). High amounts of SiO_2, Fe_xO_y, CaO and Al_2O_3 were detected (Table 1).

Table 1: Chemical composition of synthetic plasma slag (PS) according to XRF.

wt.%	SiO_2	Fe_xO_y	CaO	Al_2O_3	MgO	TiO_2	K_2O	Na_2O	CuO	MnO
PS	29.2	28.2*	26.7	13.4	0.8	0.7	0.6	0.2	0.1	0.1

*expressed as 92 % FeO and 8 % Fe_2O_3

The **IP pastes** were produced by mixing the dry milled slag with a sodium silicate activation solution in a solid to liquid ratio of 2.6 g/ml. The solution was a mixture of sodium silicate solution, sodium hydroxide pellets and distilled water (SiO_2/Na_2O molar ratio = 1.6 and H_2O/Na_2O molar ratio =20.0)[1].

Samples **cured** for 1 h, 24 h or 28 d prior to irradiation were tested. These time intervals are chosen based on the different reaction stages:

- **1 h**: minimum time after casing necessary to load the samples in the irradiation cell;
- **24 h**: right after the main reaction peak;
- **28 d**: stable and fully cured sample.

The different curing times reflect different material applications in radioactive waste management. For certain barriers, prefabricated and fully hardened materials are preferred, while for others, the material is poured close to the radioactive source(s) causing irradiation during hardening.

[1] This recipe has only been used in experiment D. For the other experiments different mix design has been used.

Different **irradiation experiments** were executed as summarized in Table 2.

Table 2: Description of the four different irradiation experiments.

	A **Low** **dose rate**	**B** **Intermediate** **dose rate**	**C** **High** **dose rate**	**D** **Very High** **dose rate**
Location	HE^2B ISIB	UHasselt	HE^2B ISIB	SCK CEN
Source	^{60}Co	^{137}Cs	^{137}Cs	^{60}Co
Energy	1.173 MeV & 1.332 MeV	0.662 MeV	0.662 MeV	1.173 MeV & 1.332 MeV
Activity	~1 TBq	35 TBq	123 TBq	unknown
Max dose rate	6.9 ± 0.15 Gy/h 1.52 ± 0.03 Gy/h	152 ± 8 Gy/h	1.25 kGy/h	8.85 kGy/h
Dose interval	0.032 kGy – 47 kGy	0.152 kGy – 95 kGy	3 kGy - 390 kGy	200 kGy
Time before irradiation	24 h or 28 d	1 h	24 h	1 h, 24 h or 28 d

For the characterization of the irradiation effects, a reference sample identical to the irradiated ones was considered for each different irradiation test. Except for the irradiation, the same procedures were applied to these reference samples:

- **Macro-mechanical strength**

  Uniaxial compressive strength tests were performed on samples of (25 x 25 x 20) mm^3 according to NBN EN 12390-3 using the Instron 5985 at a displacement of 1.0 mm/min.

- **Mercury Intrusion Porosimetry**

  MIP was performed using the Micromeritics Autopore IV 9510. Samples of (5 x 5 x 5) mm^3 were used. The samples were tested in the range of 0.01 to 414 MPa, applicable to quantify pores in the 3.6 nm to 100 µm region.

- **Fourier-transformed infrared**

  A Bruker Alpha-P with diamond crystal was used on powdered samples. 32 spectra per sample were acquired from 4000 cm^{-1} to 380 cm^{-1} at a resolution of 4 cm^{-1}. The reported spectra are the result of an average of five measurements.

- **Thermogravimetric analysis**

  TGA (TGA 550 - TA instruments) of the powdered samples was carried out from 20 °C to 1000 °C with a heating rate of 10 °C/min in a nitrogen atmosphere. The mass was measured up to 10^{-6} g precision.

- **^{57}Fe Mössbauer spectroscopy**

  Samples were powdered manually and pressed into the sample holder right before measurement. Gamma rays from a ^{57}Co source in a Rh matrix were used. The samples were measured at room temperature (RT, 300 K) in transmission geometry on a constant acceleration spectrometer. The isomer shift (IS) values are reported relative to α-Fe at RT. The IMSG software was used to fit the data [21].

Results and Discussion

Figure 1 summerizes the results of all **compressive strengths** tests executed for the different irradiation experiments. As observed, the relative strength change becomes predominantly **positive above 5 kGy** and increases further with increasing absorbed dose. Below 5 kGy on the other hand, manly a negative impact on the strength is observed. This suggests two opposing effects which work on an IP under irradiation conditions. At low dose rates and low absorbed doses the detrimental effects dominate, while for high doses (> 5 kGy) beneficial effects for the strength dominate. The effects are the strongest for IP samples only cured for 1 h (+) prior to irradiation. For the 28 d cured samples (■) on the other hand, the effects stay within the -16 % and +18 % limits, with one exception at +55 %.

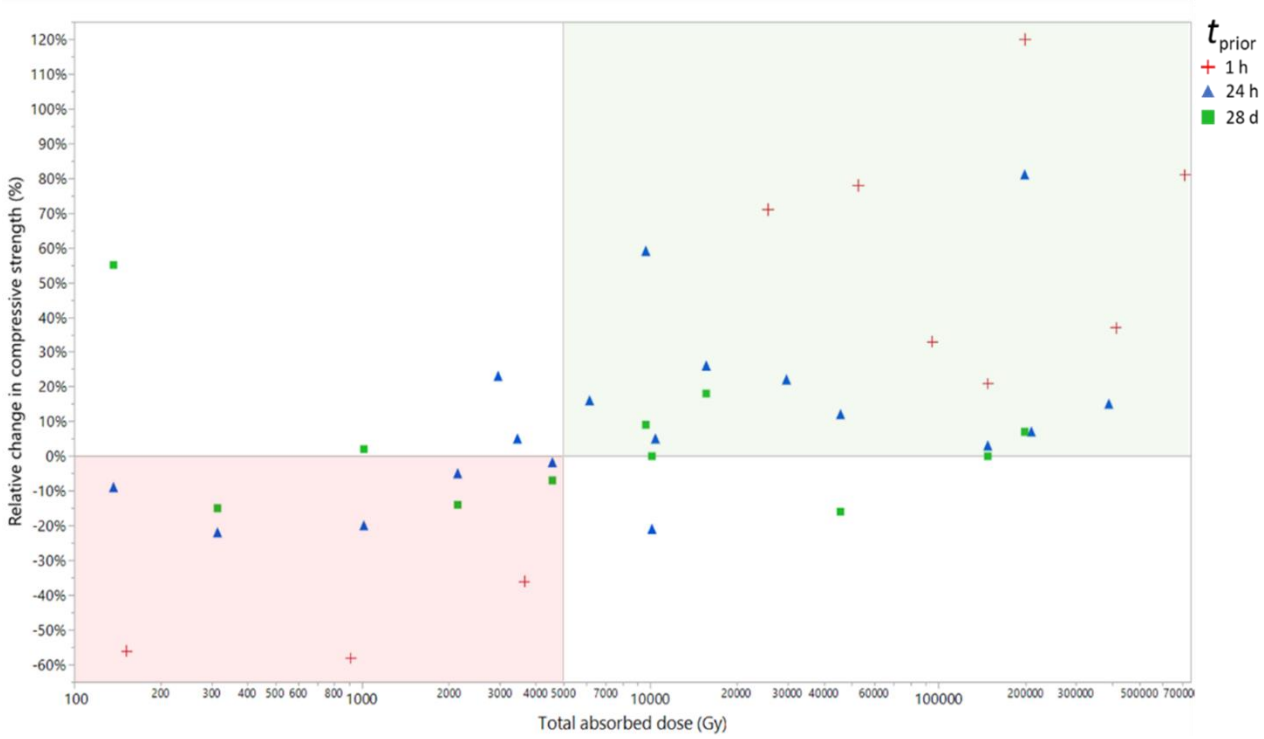

Figure 1: Overview of change in compressive strength relative to the corresponding reference, in function of the total absorbed dose for all the executed experiments.

In this document, the focus will be on the results of irradiation experiment D - 1 h cured samples. More results and details can be found in the related publications: [19], [20].

The samples irradiated at 8.85 kGy/h (D) to a total dose of 200 kGy showed in increase in strength by a factor 2.2 and a factor 1.81 for samples with t_{prior}= 1 h and t_{prior}= 24 h, respectively. For the 28 d cured samples, no significant difference was observed as a result of irradiation.

The porosity and pore size distribution (PSD) of irradiated and non-irradiated samples were determined using **MIP analysis.** The pores were mainly of the 100 - 2000 nm and < 10 nm size. The porosity for the 1 hour cured samples was significantly reduced in the 100 - 2000 nm region as result of irradiation with a shift to the smaller pore sizes. For pores smaller than 10 nm a small shift to the larger pore size diameters was detected.

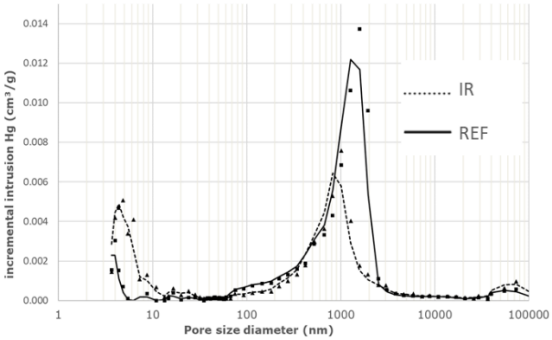

Figure 2: Pore size distribution of the irradiated samples compared to the reference samples with t_{prior}= 1 h.

Infrared spectra of the different samples did not indicate a difference as a result of irradiation. Only a small decrease in water content (3000 – 3500 cm^{-1} and from 1650 – 1655 cm^{-1}) for the irradiated samples was observed. In other irradiation experiments, radiation-altered carbonation however was observed. **TGA** results confirm the lower water content for the irradiated samples. This is related to water radiolysis during irradiation and due to the accelerated evaporation of water as a result of gamma heating. Moreover, in the region from 570 °C to 620 °C a small difference was observed. This effect is however better visible for samples irradiated over a larger time span. Therefore, the derivative thermogravimetrical curve (DTG) of a sample irradiated for 312 h at 1.25 kGy is visualized in Figure 3. A clear difference in the 400 °C to 650 °C is visible and is related to a difference in carbonates.

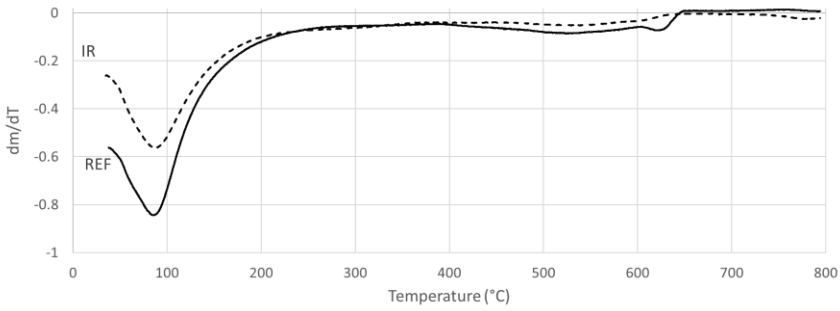

Figure 3: dm/dT curve of 24 h cured sample irradiated at 1.25 kGy/h until 624.0 kGy.

Mössbauer spectroscopy was used to determine the redox ratio of ferric (Fe^{3+}) and ferrous (Fe^{2+}) iron in the irradiated and non-irradiated IP samples. Based on the relative absorption areas the $Fe^{3+}/\sum Fe$ ratio and $Fe^{2+}/\sum Fe$ ratio was calculated. An increase in Fe^{3+} content from 20% to 39% was observed for the 1 h cured samples prior to irradiation. Strengthening of the samples can be related to the **increase in Fe^{3+} content** as a result of gamma irradiation since Fe^{3+} can take place in the silicate network [22], [23] while Fe^{2+} takes place in a trioctahedral layer [22]. Radiation-induced iron oxidation occurs as Fe^{2+} from the slag dissolution is oxidized by radiolytically produced $^{\bullet}OH$ radicals and H_2O_2. Especially in the initial reaction stage of the IP, when unbound Fe^{2+} can still be found, the effect of radiation-induced iron oxidation is expected to have the highest impact. In function of time, radiation-induced oxidation becomes more difficult as the samples dehydrate and more Fe-atoms will already be bound in the IP structure.

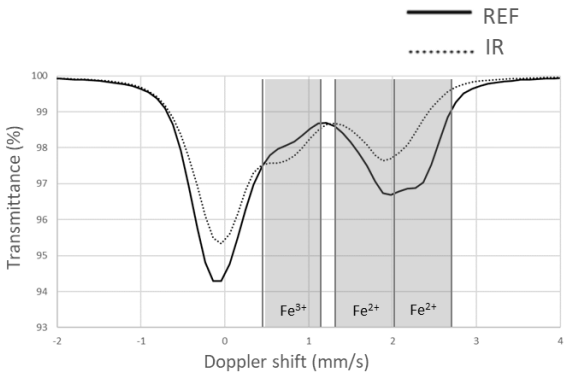

Figure 4: Comparison of the raw ^{57}Fe Mössbauer spectra of the irradiated and non-irradiated samples with t_{prior} = 1 h. The shaded areas indicate the regions of the higher velocity parts of the Fe^{3+} and the Fe^{2+} doublets used to fit the spectra.

Conclusion

1 hour cured samples are still viscous at the start of the irradiation and are therefore easily affected by gamma irradiation. As a result of gamma heating and radiolysis, water escape is promoted at the initial stage, leading to an accelerated drying and accelerated (plastic) shrinkage. Strengthening in this case can thus be related to the densification of the matrix. As water is found a crucial component in de radiation-induced Fe oxidation, a decrease in porosity favors this effect by preventing water escape from the matrix. Fe^{3+} can take place in the silicate network and contribute to the strength development of the polymer. Moreover, Fe^{2+} oxidation causes densification of the matrix which also leads to higher strength. Water retainment moreover slows down the IP reactions, thus giving irradiation effects more time to make their mark. Multiple effects were observed for the one hour cured samples: an increase of the compressive strength by a factor of 2.20, a decrease in porosity by a factor of 0.92, and an increase of the Fe3+/∑Fe ratio by a factor of 1.95. Radiation-altered carbonation was also observed.

Irradiation effects in Fe-rich IPs are complex and occur simultaneously and moreover continuously affect each other. An illustration is provided in Figure 5. The final response of the material highly depends on the absorbed dose and the state of the material at the start of the irradiation.

The mix design used in this study should be optimized when focusing on a specific application such as nuclear waste management.

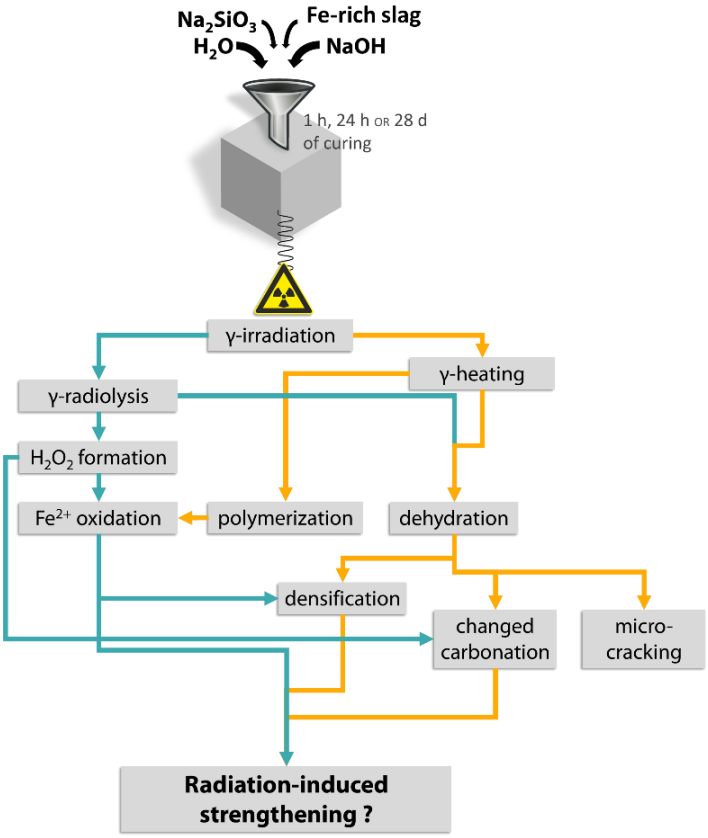

Figure 5: Radiation-induced strengthening.

Related work

1. B. Mast, Y. Pontikes, W. Schroeyers, B. Vandoren, and S. Schreurs, “The use of alkali activated materials in nuclear industry,” in *Comprehensive Nuclear Materials*, 2nd ed., R. Konings, Ed. Elsevier Inc., 2020. [13]

2. B. Mast *et al.*, “The effect of gamma radiation on the mechanical and microstructural properties of Fe-rich inorganic polymers,” *J. Nucl. Mater.*, vol. 521, 2019. [19]

3. B. Mast *et al.*, “The effect of high dose rate gamma irradiation on the curing of CaO-FeOx-SiO2 slag based inorganic polymers: Mechanical and microstructural analysis,” *J. Nucl. Mater.*, vol. in publ., 2020. [20]

References

[1] J. L. Provis and J. S. J. Van Deventer, *Alkali-Activated Materials- State-of-the-Art Report, RILEM TC 224-AAM*, vol. 13. London: Springer, 2014.

[2] J. L. Provis, “Geopolymers and other alkali activated materials: why, how, and what?,” *Mater. Struct.*, vol. 47, no. 1–2, pp. 11–25, 2014.

[3] P. Duxson, A. Fernández-Jiménez, J. L. Provis, G. C. Lukey, A. Palomo, and J. S. J. van Deventer, “Geopolymer technology : the current state of the art,” *J Mater Sci*, vol. 42, pp. 2917–2933, 2007.

[4] A. Peys, C. E. White, D. Olds, H. Rahier, B. Blanpain, and Y. Pontikes, “Molecular structure of CaO – FeOx – SiO2 glassy slags and resultant inorganic polymer binders,” *J. Am. Ceram. Soc.*, vol. 101, no. 12, pp. 5846–5857, 2018.

[5] J. L. Provis and J. S. J. van Deventer, Eds., *Geopolymers: structure, processing, properties and industrial applications*, 1st ed. Cambridge: Woodhead Publishing Limited, 2009.

[6] P. Krivenko, “Why alkaline activation - 60 years of the theory and practice of alkali-activated materials,” *J. Ceram. Sci. Technol.*, vol. 8, no. 3, pp. 323–333, 2017.

[7] J. G. S. Van Jaarsveld, J. S. J. Van Deventer, and L. Lorenzen, “Potential use of geopolymeric materials to immobilize toxic metals: Part I. Theory and applications,” *Miner. Eng.*, vol. 10, no. 7, pp. 659–669, 1997.

[8] International Atomic Energy Agency, “The Behaviours of Cementitious Materials in Long Term Storage and Disposal of Radioactive Waste : Results of a Coordinated Research Project.,” Vienna, 2013.

[9] F. Chupin, A. Dannoux-papin, Y. N. Ravache, and J.-B. D’Espinose de Lacaillerie, “Water content and porosity effect on hydrogen radiolytic yields of geopolymers,” *J. Nucl. Mater.*, vol. 494, pp. 138–146, 2017.

[10] J. Davidovits, “Geopolymer, Green Chemistry and Sustainable Development Solutions,” in *Proceedings of the World Congress Geopolymer 2005*, 2005, p. 236.

[11] N. Vandevenne *et al.*, “Incorporating Cs and Sr into blast furnace slag inorganic polymers and their effect on matrix properties,” *J. Nucl. Mater.*, vol. 503, pp. 1–12, 2018.

[12] P. Duan, C. Yan, W. Zhou, W. Luo, and C. Shen, “An investigation of the microstructure and durability of a fluidized bed fly ash–metakaolin geopolymer after heat and acid exposure,” *Mater. Des.*, vol. 74, pp. 125–137, 2015.

[13] B. Mast, Y. Pontikes, W. Schroeyers, B. Vandoren, and S. Schreurs, “The use of alkali activated materials in nuclear industry,” in *Comprehensive Nuclear Materials*, 2nd ed., R. Konings, Ed. Elsevier Inc., 2020.

[14] T. Croymans-Plaghki, “Valorization of Fe-rich industrial by-products in construction materials: a radiological assessment,” UHasselt, 2018.

[15] R. P. Williams and A. van Riessen, “Development of alkali activated borosilicate inorganic polymers (AABSIP),” *J. Eur. Ceram. Soc.*, vol. 31, no. 8, pp. 1513–1516, 2011.

[16] H. Takeda, S. Hashimoto, H. Matsui, S. Honda, and Y. Iwamoto, “Rapid fabrication of highly dense geopolymers using a warm press method and their ability to absorb neutron irradiation,” *Constr. Build. Mater.*, vol. 50, pp. 82–86, 2014.

[17] L. Machiels, L. Arnout, P. Yan, P. Tom Jones, B. Blanpain, and Y. Pontikes, “Transforming Enhanced Landfill Mining Derived Gasification / Vitrification Glass into Low-Carbon Inorganic Polymer Binders and Building Products,” *J. Sustain. Metall.*, vol. 3, no. 2, pp. 405–415, 2016.

[18] European Comittee for standardization, “EN 196-6:2010 - Methods of testing cement - Part 6: Determination of fineness,” pp. 1–18, 2010.

[19] B. Mast *et al.*, “The effect of gamma radiation on the mechanical and microstructural properties of Fe-rich inorganic polymers,” *J. Nucl. Mater.*, vol. 521, 2019.

[20] B. Mast *et al.*, “The effect of high dose rate gamma irradiation on the curing of CaO-FeOx-SiO2 slag based inorganic polymers: Mechanical and microstructural analysis,” *J. Nucl. Mater.*, vol. in publ., 2020.

[21] P. Douvalis, A. Polymeros, and T. Bakas, “IMSG09: A 57Fe -119Sn Mössbauer spectra computer fitting program with novel interactive user interface,” *J. Phys. Conf. Ser.*, vol. 217, no. 1, 2010.

[22] A. Peys, A. P. Douvalis, V. Hallet, H. Rahier, B. Blanpain, and Y. Pontikes, “Inorganic Polymers From CaO-FeOx-SiO2 Slag: The Start of Oxidation of Fe and the Formation of a Mixed Valence Binder,” *Front. Mater.*, vol. 6, no. 212, pp. 1–10, 2019.

[23] P. N. Lemougna, K. J. D. Mackenzie, G. N. L. Jameson, and H. R. U. F. Chinje, “The role of iron in the formation of inorganic polymers (geopolymer) from volcanic ash : a 57Fe Mössbauer spectroscopy study,” *J. Mater. Sci.*, vol. 48, pp. 5280–5286, 2013.